Transport capacity and saturation mechanism in a cellular automaton dune model.

ZHANG Deguo, GAO Xin, ROZIER Olivier & NARTEAU Clément
Institut de Physique du Globe de Paris
Sorbonne Paris Cité, Univ Paris Diderot, UMR 7154 CNRS
1 rue Jussieu, 75238 Paris, Cedex 05, France.

ABSTRACT: In a lattice gas cellular automaton dune model, individual physical processes such as erosion, deposition and transport are implemented by nearest neighbor interactions and a time-dependent stochastic process. As a consequence, local sediment fluxes are not defined by a set of equations that incorporates the effect of flow and dune shape on transport capacity. Instead, there is a dynamic equilibrium between the topography, the flow and the sediment in motion that reduces the basal shear stress at the surface of the bed. Then, the saturation flux, the saturation length and the characteristic wavelength for the formation of dunes are emergent properties that can be estimated a posteriori from the numerical outputs. Here, we propose a simplified version of the model to establish asymptotic relationships between the microscopic erosion-deposition-transport rate parameters and the characteristic length and time scale of the flux saturation mechanism. Then, we discuss how we can use our results to determine the rate parameters of cellular automaton models that study the effect of heterogeneities in grain-size distribution on dune morphodynamics.

1 INTRODUCTION

There are two main types of numerical experiments for the modeling of bed forms:

- Continuous models are based on a set of partial differential equation that combine the principle of mass conservation with analytical descriptions of the flow and transport capacity (Sauermann et al., 2001; Kroy et al., 2002; Andreotti et al., 2002; Fischer et al., 2008). Their main advantage is related to the dimensionality of the system. Nevertheless, in such a continuous-homogeneous framework, it remains difficult to evaluate how the deterministic nature of specific ingredients affect the overall dynamics (e. g. effect of curvature, flow separation, recirculation eddies).
- Cellular automaton models are discrete models that implement a set of rules to mimic sediment transport and the effect of the flow on topography *(*Nishimori and Ouchi, 1993; Werner and Gillespie, 1993; Werner, 1995*)*. Their main advantage is that they reproduce a huge variety of bed forms at a reasonable computational cost. Nevertheless, they are constructed from an arbitrary elementary length-scale which is not always related to other characteristic length-scale of the problem.

The real-space cellular automaton dune model developed by Narteau et al., (2009) is an attempt to overcome these problems. If it belongs to the class of discontinuous models, its characteristic length a time scales have been entirely defined with respect to a linear stability analysis. This standard technique (used in many other branches of physics) identifies stable/unstable regimes across the entire parameter space of the model to reveal the mechanisms that, starting from a flat sand bed, spontaneously generate

bed forms. As a result, we can quantitatively compare our numerical results to observations in nature and laboratory experiments, as well as to the predictions of other modeling techniques (Zhang et al., 2010).

The real-space cellular automaton dune model is a hybrid approach that combines a cellular automaton of sediment transport with a lattice-gas cellular automaton for high Reynolds-flow simulation (Frisch et al., 1986, d' Humières et al., 1986). At the elementary length scale l_0 of this cellular automaton, all the physical mechanisms are implemented by nearest neighbour interactions and a time-dependent stochastic process. In practice, there is a finite number of transitions associated with erosion, transport and deposition. Each set of transition being characterized by a rate parameter $\Lambda_{\{e,t,d\}}$ with unit of frequency $1/t_0$, we incorporate into the model the characteristic time scales of the physical processes under consideration.

In all natural environments where the dune instability can be observed, this model can be used by setting the length and time scales $\{l_0, t_0\}$ to the appropriate values of the relevant physical parameters. Thus, we can set up the model to reproduce aeolian or subaqueous dune features on Earth and other planetary bodies (Claudin and Andreotti, 2006). For example, in units of the model, the barchan dune presented in Fig. 1 has a height of 25 l_0 and a propagation speed of 0.028 l_0/t_0. In arid desert on Earth for a grain size d=200 µm, it corresponds to a dune height of 12.5 m and a propagation speed of 17.5 m/yr; in water, it corresponds to a dune height of 1.3 cm and a propagation speed of 10 m/h; on Mars for a grain size d=87 µm, it corresponds to a dune height of 375 m and a propagation speed of 9 cm/yr.

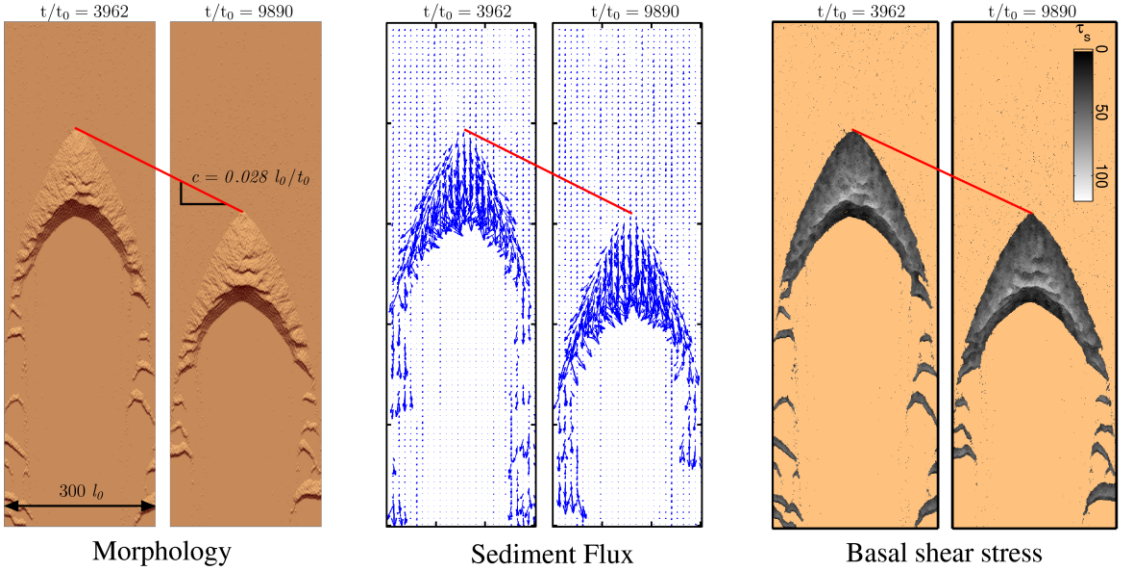

Figure 1 Morphodynamics of a barchan in the lattice gas cellular automaton dune model. **(a)** Morphology of the barchan at t/t_0=4063 and t/t_0=7011. Note the presence of superimposed bed forms. **(b-c)** Sedimentary fluxes and basal shear stress on the barchan (see Narteau et al., (2009) and Zhang et al., (2010) for details about the model).

Here, our goal is to quantify the saturated flux and the saturation length of our model with respect to the transition rates that characterize the mechanisms of erosion, transport and deposition at the elementary length scale of the cubic lattice. Such analytical relationships are critical to incorporate into the model a real-space representation of heterogeneous granular systems: particle size distributions, variability in particle density as well as the role of cohesion and vegetation.

2 A SIMPLIFIED REAL SPACE CELLULAR AUTOMATON MODEL

To measure sediment flux in the model, we adopt here the experimental protocol proposed by Bagnold, (1941). As shown in Fig. 2, the initial condition is a thick flat layer of sediment preceded, in the direction of the flow, by a non-erodible flat bed. Then, the sediment load increases as the flow reaches the erodible bed. The principle of the experiment consists in measuring sediment flux as a function of distance in the direction of flow. In practice, this experience is extremely difficult to implement in situ or in laboratory experiments because it is difficult to maintain a flat sediment bed over long time scales. The two main reasons are (a) the formation/migration of an erosion front at the discontinuity from non-erodible to erodible bed and (b) the formation of sedimentary structures such as ripples or dunes. The same problem exists in our simulations. It is even more pronounced because of the ratio between our elementary scale (l_0=0.5 m) and the grain size in nature (d=200 µm). Indeed, the amplitude of the smallest surface roughness plays against us in the model. Fortunately, our numerical approach offers the opportunity to overcome this obstacle.

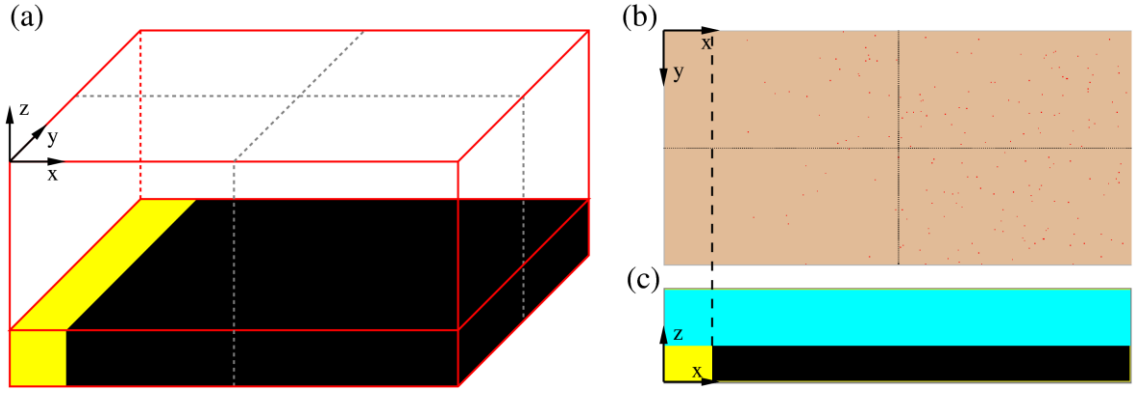

Figure 2 **(a)** Initial condition of the cellular automaton. Fluids cells (cyan) and neutral cells (yellow) that make up the ceiling are transparent for the sake of readability. **(b)** Distribution of mobile sedimentary cells (red) when the system reaches a dynamic equilibrium state. Note the increasing number of mobile sedimentary cells in the direction of the flow. Their size gives the elementary length scale l_0. The dashed line indicates the limit between the non-erodible and the erodible bed. **(c)** A vertical slice of cells in the direction of the flow. Note the presence of the ceiling that confines the flow.

To eliminate the influence of bed topography on the flow, we simplify the cellular automaton of sediment transport using the same three states (fluid, immobile sediment, sediment in motion) but only three transitions (Fig. 3). This new set of transitions has the advantage to preserve the initial bed topography composed of stable cells. Nevertheless, these transitions violate the principle of mass conservation if the mobile sedimentary cells have a non-null density. In the following, we therefore arbitrarily consider that the mass of mobile sedimentary cells is null. Conceptually, we should admit that, when a sediment cell becomes mobile, it is immediately replaced by a stable sediment cell with exactly the same properties. By symmetry, when a mobile sediment cell becomes stable, it is immediately removed from the surface of the bed. Then, the flow is only disturbed by sediment transport and it is not affected by changes in bed topography. In this case, we can focus on the saturation mechanism by studying the evolution of shear stress as well as the screening/armouring effect produced by the mobile sedimentary cells.

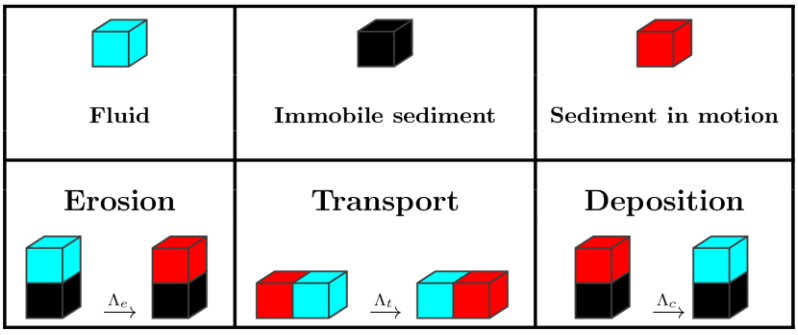

Figure 3 Active transitions of doublets in the simplified cellular automaton model for sediment transport. Different transitions are associated with erosion, transport and deposition. Transition rates with units of frequency are Λ_e, Λ_t, Λ_d.

Overall, the simplicity of this new cellular automaton of sediment transport also allows us to derive (and numerically verify) a number of analytical relationships involving Λ_e, Λ_t, Λ_d, the rate parameters of the model.

3 SATURATION LENGTH AND SATURATED FLUX

At the beginning of each simulation, we stabilize the flow. As a result, the basal shear stress is statistically constant across the entire domain. Then, we activate the transitions of doublets (Fig. 2) incrementing the time for each of them (see Appendix B in Narteau et al., (2009)). In vertical planes perpendicular to the flow, we systematically count the total number of transport transitions to average the sediment flux over the entire width of the domain. Fig. 4a shows the sediment flux with respect to distance downstream for $\Lambda_e t_0 = 4.10^{-5}$, $\Lambda_t t_0 = 50$, $\Lambda_d t_0 = 2$. Above the erodible area (i.e. $x > x_0 = 50\ l_0$), we observe that the flow relaxes to an equilibrium value Q_{sat} over a characteristic distance l_{sat}. The quality of the approximation by a law of the form

$$Q(x) = Q_{sat}\left(1-\exp\left(-\frac{x-x_0}{l_{sat}}\right)\right)$$

shows that we have an exponential relaxation process. We discuss below the Q_{sat} and l_{sat}-values according to the parameters of the model.

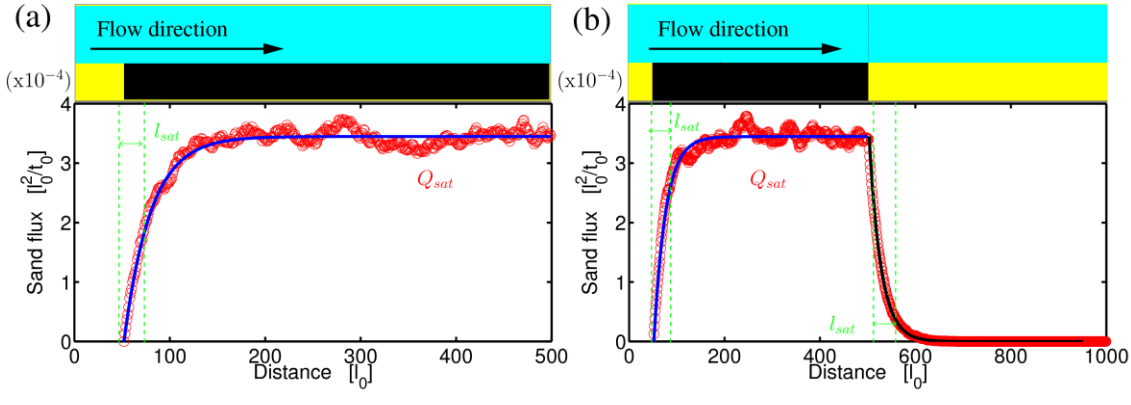

Figure 4 Saturation length and saturated flux in the simplified cellular automaton model. **(a)** Downstream of the transition from a non-erodible to an erodible bed, the sediment flux adjusts to the basal shear stress and reaches a stable value Q_{sat} over a characteristic distance l_{sat}. **(b)** Charge and discharge mechanisms follow the same exponential relaxation regime (see blue/black lines).

To better understand the origin of the l_{sat}-value in our model, we take the same initial condition as in the previous numerical experiment (Fig. 4a), but add a non-erodible zone downstream. Fig. 4b shows how the sediment load returns to zero when the flow reaches the non-erodible zone at $x_1 = 500\ l_0$. Not surprisingly, a law of the form

$$Q(x) = Q_{sat} \exp\left(-\frac{x-x_1}{l_{sat}}\right)$$

fits very well the evolution of sediment flux for $x>x_1$. Once again, we find that the sediment load relaxes towards its equilibrium value over the characteristic distance l_{sat}. The increase and the decrease of the sediment load follow the same exponential process. Therefore, we conclude that, in our simplified cellular automaton model, the saturation length is the mean distance over which a mobile sedimentary cell is transported.

Let us consider that the average distance X traveled by a mobile sedimentary cell is a discrete random variable with probability density function f. Then, we can write

$$l_{sat} = \langle X \rangle = \sum_{X=0}^{\infty} X f(X)$$

In the model, a mobile sedimentary cell moves if it participates in a transition of transport. It becomes stable if it participates to a transition of deposition. For a given mobile sedimentary cell, these two transitions occur with probabilities

$$P_t = \frac{\Lambda_t}{\Lambda_t + \Lambda_d} \quad \text{and} \quad P_d = \frac{\Lambda_d}{\Lambda_t + \Lambda_d}$$

Then, from the probability tree of the dynamics of a mobile sedimentary cell, we obtain

$$f(X) = P_t^X (1-P_t) = P_t^X P_d$$

By injecting these last three relations in the expression of l_{sat}, we obtain

$$l_{sat} = \sum_{X=1}^{\infty} X P_t^X (1-P_t) = l_0 \sum_{X=1}^{\infty} P_t^X = \frac{P_t}{1-P_t} l_0 = \frac{\Lambda_t}{\Lambda_d} l_0$$

Thus, we show that the saturation length is directly the ratio between the characteristic time for deposition and the characteristic time for transport. For a given flow rate, this dependence on deposition and erosion is exactly the same as for many continuous models (Charru, 2006). Fig. 5 shows that the numerical solutions verify the analytical solution.

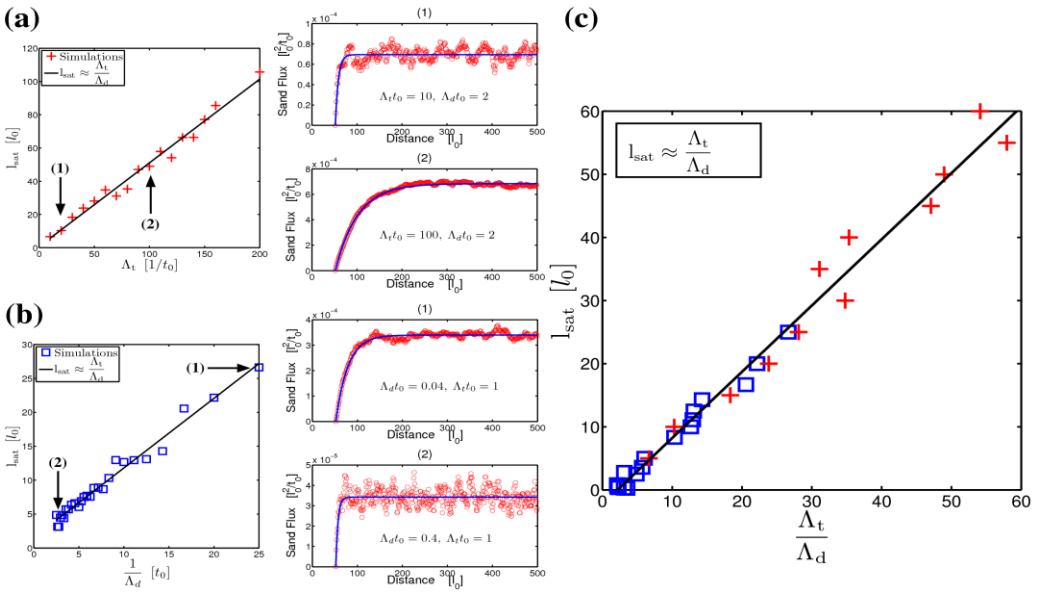

Figure 5 Relation between l_{sat} and the rate parameters of the cellular automaton model. **(a)** l_{sat} with respect to Λ_t for $\Lambda_d t_0$=2. Two examples show the sediment flux for (1) $\Lambda_t t_0$ =10 and (2) $\Lambda_t t_0$ =100. **(b)** l_{sat} with respect to $1/\Lambda_d$ for $\Lambda_t t_0$=1. Two examples show the sediment flux for (1) $\Lambda_d t_0$ =0.04 and (2) $\Lambda_d t_0$ =0.4. **(c)** l_{sat} with respect to Λ_t/Λ_d, the mean distance traveled by a mobile sedimentary cell.

The saturated sediment flux Q_{sat} is the number of transition of transport at a given point. This number depends only on a transition of erosion upstream followed by a sufficient number of transitions of transport. In all respects, the saturated flow can be written

$$\frac{Q_{sat}}{l_0^2} = \sum_{X=1}^{\infty} \Lambda_e P_t^X = \Lambda_e \frac{P_t}{1-P_t} = \frac{\Lambda_e \Lambda_t}{\Lambda_d}$$

This formula shows that the saturated flow is the direct product of the erosion rate by the average distance traveled by a mobile sedimentary cell. Fig. 6 shows that the numerical solutions verify this analytical solution.

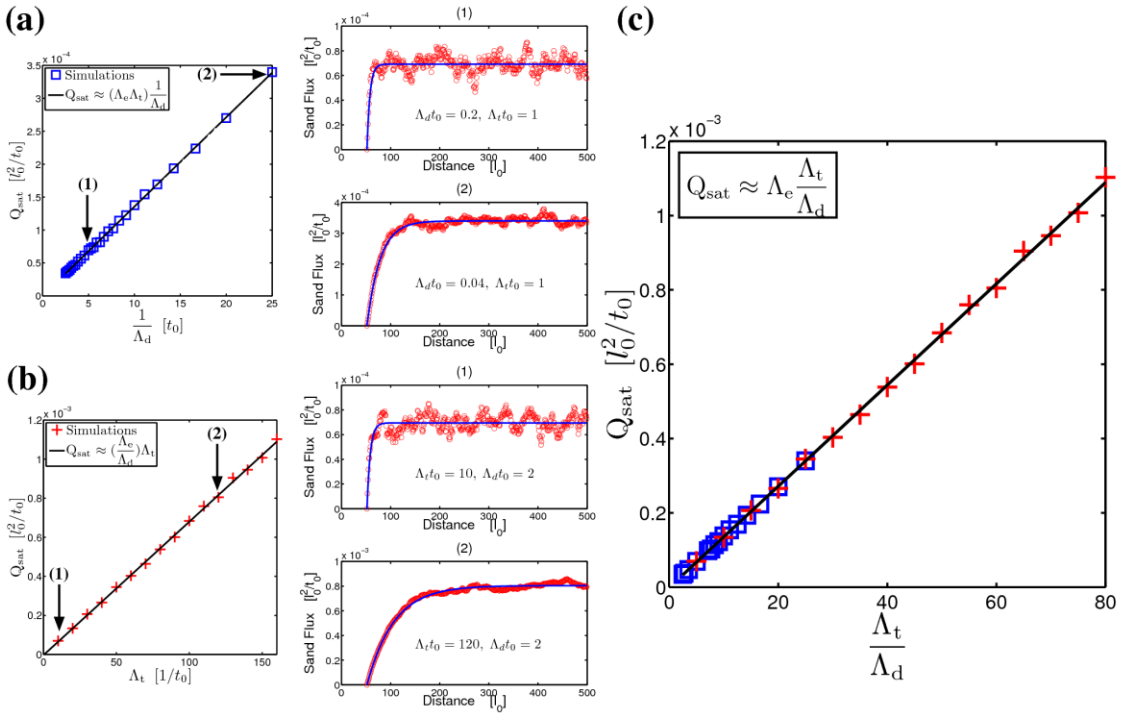

Figure 6 Relation between Q_{sat} and the rate parameters of the cellular automaton model. **(a)** Q_{sat} with respect to $1/\Lambda_d$ for $\Lambda_t t_0$=1. Two examples show the sediment flux for (1) $\Lambda_d t_0$ =0.2 and (2) $\Lambda_d t_0$ =0.04. **(b)** Relation between Q_{sat} and Λ_t for $\Lambda_d t_0$=2. Two examples show the sediment flux for (1) $\Lambda_t t_0$ =10 and (2) $\Lambda_t t_0$ =120. (c) Q_{sat} with respect to Λ_t/Λ_d, the mean distance traveled by a sedimentary cell. The slope of this relationship is proportional to Λ_e.

4 THE SATURATION TIME AND THE DENSITY OF MOBILE SEDIMENTARY

The sediment flux does not adjust immediately to its local Q_{sat}-value. It always takes some time to reach this dynamic equilibrium state. To estimate this time, we can count the number N_m of mobile cells on the erodible bed. These mobile cells protect the bed from further erosion. More exactly, because they cannot move vertically, they prevent erosion of cells that compose the flat erodible bed just below them. Then, if N_s is the number of erodible cells exposed to the flow, we can write

$$\begin{cases} \dfrac{dN_m}{dt} = -\Lambda_d N_m + \Lambda_e N_s \\ \dfrac{dN_s}{dt} = \Lambda_d N_m - \Lambda_e N_s \end{cases}$$

This is a system of coupled linear equations with solution of the form $\exp(\lambda t)$. The eigenvalues can be found by solving

$$(\Lambda_d + s)(\Lambda_e + s) - \Lambda_e \Lambda_d = s^2 + s(\Lambda_d + \Lambda_e) = 0$$

The only non-zero solution is equal to $-(\Lambda_e+\Lambda_d)$. As a consequence, the number of mobile sedimentary cell in the system relaxes exponentially to its equilibrium value over a characteristic time

$$t_{sat} = \frac{1}{\Lambda_d + \Lambda_e}$$

With Fig. 7, we verify numerically this exponential relaxation process at all location downstream of the transition from a non-erodible to an erodible bed.

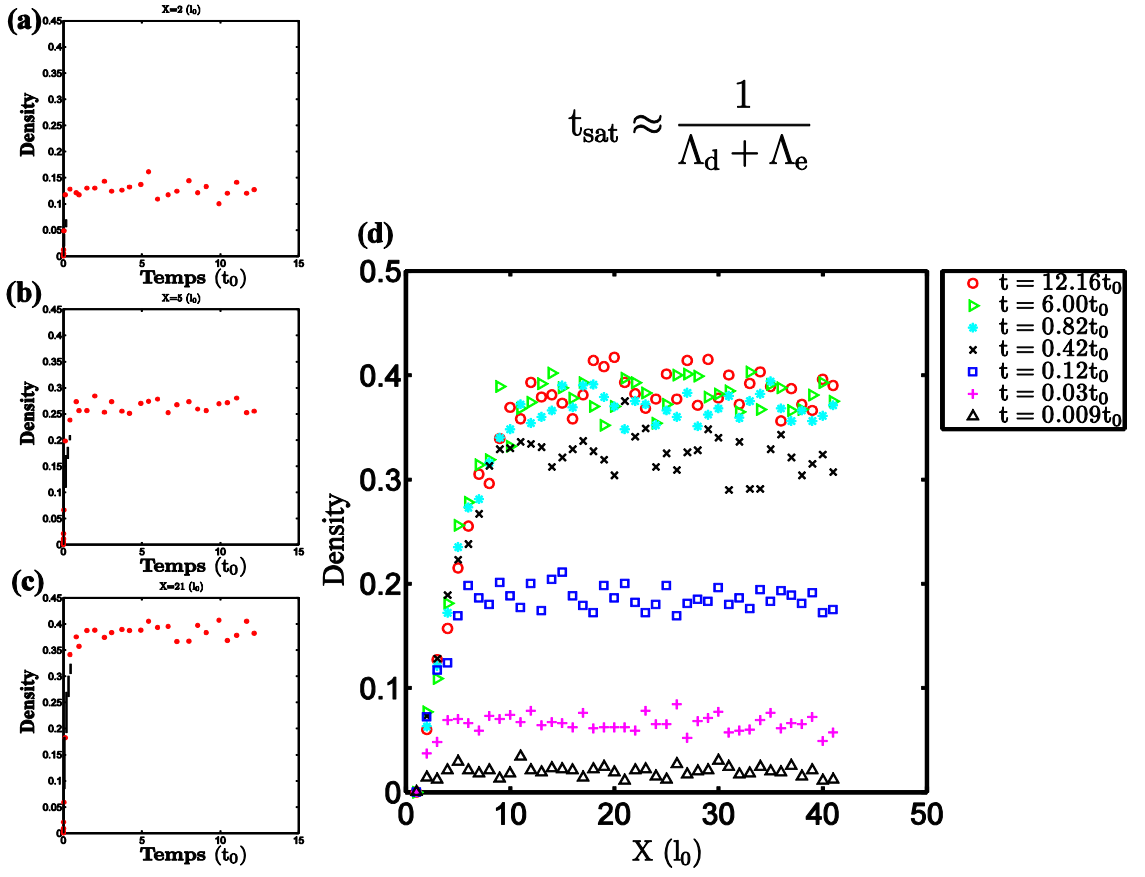

Figure 7 Relation between the saturation time t_{sat} and the rate parameters of the cellular automaton model. **(a-c)** Density of mobile sedimentary cells in vertical plane perpendicular to the flow at *x={2, 5, 21}* with respect to time. *x* is expressed in units of l_0 and *x=0* is the transition from a non-erodible to an erodible bed. **(d)** Density of mobile sedimentary cells in vertical plane perpendicular to the flow with respect to *x* for different times.

Finally, the equilibrium solution of our system of coupled linear equations is simply

$$\frac{N_m}{N_s} = \frac{\Lambda_e}{\Lambda_d}$$

Since the density of mobile cell on the bed can be written

$$d_s = \frac{N_s}{N_s + N_m}$$

we have

$$d_s = \frac{\Lambda_e}{\Lambda_e + \Lambda_d}$$

With Fig. 8, we verify numerically this relationship within this simplified version of the cellular automaton dune model.

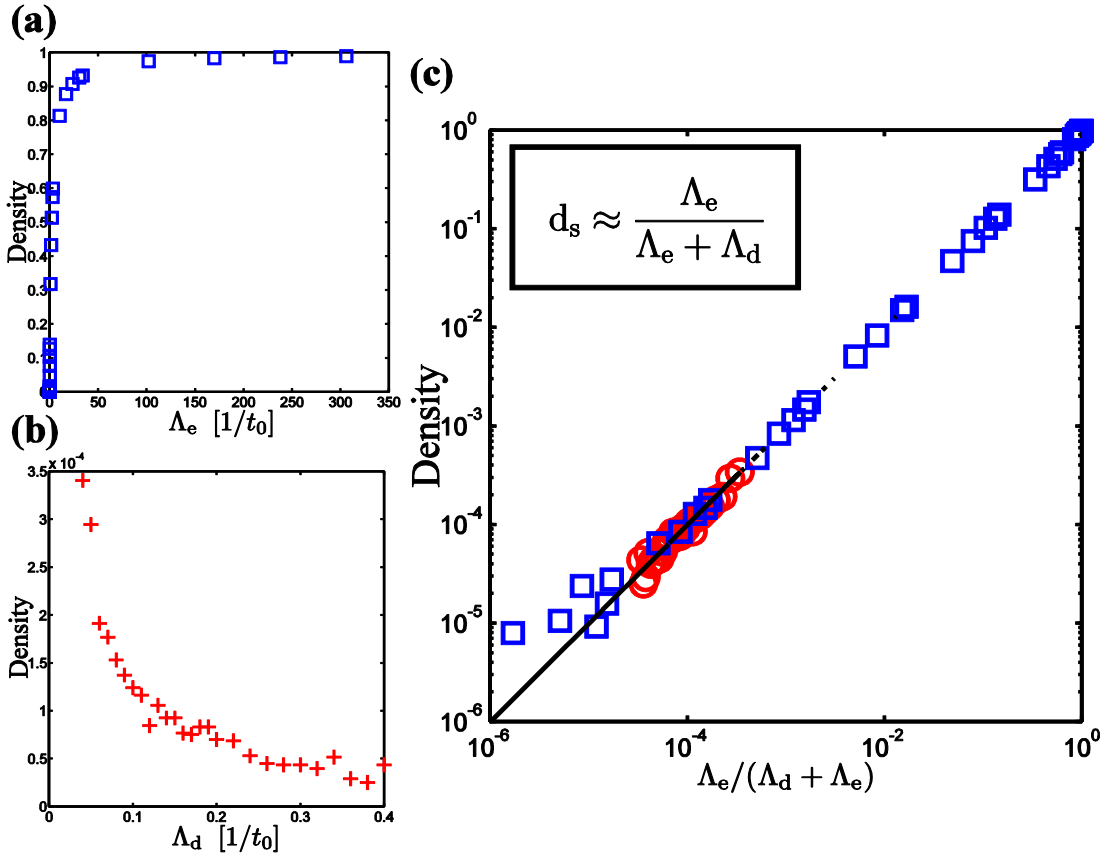

Figure 8 Relation between the density of mobile sedimentary cells on the bed and the rate parameters of the cellular automaton model. **(a)** Density of mobile sedimentary cells with respect to Λ_e for $\Lambda_d t_0$ =2. **(b)** Density of mobile sedimentary cells with respect to Λ_d for $\Lambda_e t_0$ =4.10^{-5}. **(b)** Density of mobile sedimentary cells with respect to $\Lambda_e/(\Lambda_e+\Lambda_d)$.

5 CONCLUDING REMARKS

From the outputs of this simplified version of the model, we are now able to infer the Q_{sat} and l_{sat}-values of the cellular automaton dune model (Narteau et al., 2009, Zhang et al., 2010). We show that these values depend directly on the rate parameters that characterize the erosion-deposition-transport process at the elementary length scale of the cubic lattice. This is of primary importance in determining the characteristic length scale for the formation of dunes in monodisperse granular system. In addition, we can play with our parameterization to compare the results of our simulations with predictions of theoretical models and results of field and laboratory experiments (Elbelrhiti et al., 2005; Andreotti et al., 2008).

In order to study polydisperse granular beds with the cellular automaton dune model, different transition

rates can be assigned to different granular states. In this case, we can use the results presented here to constrain the value of these transition rates with respect to the physical properties of the granular medium (density, grain size). For example, we can take

$$\Lambda_d \sim \sqrt{\frac{\Delta \rho g}{d}} \quad \text{and} \quad \Lambda_e \sim \frac{\tau_0}{\rho_g \sqrt{\Delta \rho g}\, d^{3/2}}$$

where τ_0 has units of shear stress, d is the grain diameter, $\Delta\rho=(\rho_g-\rho_f)/\rho_f$ and ρ_g and ρ_f are the grain and the fluid density, respectively. In addition, it will be necessary to incorporate dependence on the strength of the flow for the magnitude of Λ_t. At the microscopic length scale, Lajeunesse et al. (2010) has shown that this dependence can take different forms according to the speed of moving grains at the threshold of motion inception.

In our cellular automaton, when the density of mobile sedimentary cell increases (Fig. 8), it happens more and more frequently that two of them are aligned in the direction of flow. Such a configuration prevents the occurrence of a transport transition for the upstream mobile sedimentary cell. So, there is a feedback of the number of mobile sedimentary cell on transport properties. If this feedback takes different form (see the paragraph below), it is important to note that our analytical expression of Q_{sat} and l_{sat} are only valid when the probability to have transport transitions is not affected by the number of mobile sedimentary cells. To overcome this problem, it is easy to create a dependency between vertical motions of mobile sedimentary cells and their number. Nevertheless, this is a new level of complexity which is unnecessary for dune morphodynamics since $d_s < 0.1$ across the entire domain.

Even in this simplified model, there is a retroaction of the sediment in motion on the flow and transport properties. First, mobile sedimentary cells create a dynamical armoring of the bed that prevents for further transition of erosion just below them. Second, they also reduce the basal shear stress by increasing the roughness of the sedimentary layer. This second effect has not been studied here because it requires more realistic trajectories for mobile sedimentary cells.

Finally, the comparison between our estimates and Q_{sat} and l_{sat} and theoretical models such as the one developed by Charru, 2006 allows us to better understand the ingredients that need to be incorporate into our cellular automaton approach to describe transport properties at the length scale of a grain.

REFERENCES

Andreotti, B., P. Claudin, & S. Douady (2002), Selection of dune shapes and velocities – part 1: Dynamics of sand, wind and barchans, Euro. Phys. J. B., 28 (3), 321–339.

Andreotti, B., P. Claudin, & O. Pouliquen (2010), Measurements of the aeolian sand transport saturation length, Geomorphology, 123 (3-4), 343–348.

Bagnold, R. A. (1941), The physics of blown sand and desert dunes, Methuen, London.

Charru, F. (2006), Selection of the ripple length on a granular bed, Phys. Fluids, 18, 121–508.

Claudin, P., & B. Andreotti (2006), A scaling law for aeolian dunes on Mars, Venus, Earth, and for subaqueous ripples, Earth. Planet. Sci. Lett., 252 (1-2), 30–44.

d'Humières, D., P. Lallemand, & U. Frisch (1986), Lattice gas models for 3d hydrodynamics, Europhys. Lett., 2 (4), 291–297.

Elbelrhiti, H., P. Claudin, & B. Andreotti (2005), Field evidence for surface-wave-induced instability of sand dunes, Nature, 437, 720–723. 1

Fischer, S., M. E. Cates, & K. Kroy (2008), Dynamic scaling of desert dunes, Phys. Rev. E, 77 (3), 031,302.

Frisch, U., B. Hasslacher, & Y. Pomeau (1986), Lattice-gas automata for the navier-stokes equation, Phys. Rev. Lett., 56 (14), 1505–1508.

Kroy, K., G. Sauermann, & H. J. Herrmann (2002), Minimal model for sand dunes, Phys. Rev. Lett., 88 (5).

Narteau, C., D. Zhang, . Rozier, & P. Claudin (2009), Setting the length and time scales of a cellular automaton dune model from the analysis of superimposed bed forms, J. Geophys.Res., 114, F03006.

Nishimori, H., & N. Ouchi (1993), Computational models for sand ripple and sand dune formation, Int. J. Mod. Phys. B, 7 (9-10), 2025–2034, workshop on dynamics of power systems, Tokyo, Japan, Nov 16-18, 1992. 1

Sauermann, G., K. Kroy, & H. J. Herrmann (2001), Continuum saltation model for sand dunes, Phys. Rev. E, 64 (3, Part 1), art. no.–031,305. 1

Werner, B. T. (1995), Eolian dunes: Computer simulations and attractor interpretation, Geology, 23, 1107. 1

Werner, B. T., & D. T. Gillespie (1993), Fundamentally discrete stochastic model for wind ripple dynamics, Phys.

Rev. Lett., 71, 3230. 1
Zhang, D., C. Narteau, & Rozier (2010), Morphodynamics of barchan and transverse dunes using a cellular automaton model, J. Geophys. Res., 115.